A Modified LCC-Compensated Pickup Topology for Dynamic Wireless Power Transfer Systems

Mattia Forato, *Student Member, IEEE*, Manuele Bertoluzzo
Department of Industrial Engineering, University of Padova, Padova, Italy
mattia.forato@studenti.unipd.it, manuele.bertoluzzo@unipd.it

***Abstract* — This paper proposes an unconventional pickup topology employed in the dynamic battery charging of electric vehicles. The pickup reactive power compensation is performed through a modified LCC network that permits the continuous conduction mode operation of the rectifier for a wide range of working conditions. The dc/dc converter that controls the battery charging process requires a small value of dc inductance for the proper operation. The proposed control strategy for the switch in the dc/dc conversion stage maintains the pickup input power factor close to one for large variations of the charging power. In this paper, at first the operation of the proposed topology and its related control strategy are introduced and then a design procedure for the modified LCC network parameters is presented. The pickup topology is implemented in PSIM and the outcomes of the simulations corroborate the analytical analysis.**

***Keywords* — Wireless Power Transfer (WPT), Dynamic WPT (DWPT), LCC compensation network, DWPT control.**

I. INTRODUCTION

The growing concerns about the environmental pollution and the depletion of the fossil reservoirs have led to a worldwide interest in electric mobility [1]. Although Hybrid Electric Vehicles (HEVs) and Plug-In Hybrid Electric Vehicles (PHEVs) are already a viable solution for the consumers in the cars market, pure Electric Vehicles (EVs) need to overcome the questions of the limited driving range and the long charging time to be widely accepted [2].

Dynamic Wireless Power Transfer (DWPT) is an emerging technology that allows a moving EV to be charged from an external stationary grid, by means of an inductive power transfer. The advantage introduced by the DWPT is that constraints on EVs storage can be relaxed since a portion of the traction and charging power is delivered by the grid [3], [4].

In a DWPT system (DWPTS) several transmitting coils, supplied with a high-frequency current, are deployed under the roadway pavement to form the track. A receiving coil, known as pickup, is installed underneath the EV. When the EV moves along the road, the pickup coil intercepts the magnetic flux produced by the track and, according to Faraday's law, a voltage appears at its terminals [5]. The induced voltage is conditioned by a compensation network, a rectifier and a dc/dc converter prior to charging the battery.

The large variation of the coil coupling and the different levels of power required by the battery at various State Of Charge (SOC) make the control of DWPTSs a tough task [6]. Among all the possible control strategies [7], the easiest and the most feasible seems to be the secondary-side control, also known as decoupling control [8]. In this control strategy, the current of the track coil directly coupled with the pickup is maintained constant, whereas a dc/dc converter in the receiving-side is responsible for performing the battery charging regulation. The controller that acts to maintain the track current constant does not use information regarding the receiver operation, thus eliminating the need for a feedback communication.

There are several possible topologies of dc/dc converters usable in the pickup-side to regulate the battery charging [9]. All of them require a large dc inductance for the proper operation. This bulky component can be eliminated or at least significantly reduced using a full bridge rectifier and implementing the power regulation at this stage [10]. However, when the bidirectional power flow is not necessary, this solution adds complexity and cost. In [11], the receiving-side control is implemented by employing a semi-active rectifier. With the proposed control method, the two switches are softly commutated, but the phase displacement between the receiving voltage and current depends on the switch control angle and, in the case of a DWPTS, a Unity Power Factor (UPF) cannot be guaranteed. In [12], the authors introduce an LCL-compensated pickup with a slow-controlled switch inserted directly after the diode bridge without the need for the dc inductance typical of the parallel compensation used to sustain the rectifier output current. Such a controller, valid for material handling systems, does not have the high-speed performance required in a DWPTS.

In this paper the topology presented in [12] is revised and a different control strategy is proposed in order to fulfil the stringent requirements of a DWPTS. The particular control strategy allows a UPF to be maintained at the input of the receiver for a wide range of the operating conditions, thus improving the pickup sizing factor. More in detail, the paper is organized as follows. The analysed pickup topology is introduced in Section II and its operation is presented in Section III. In Section IV, a sizing procedure for the components of the pickup compensation network is provided. The analysed topology with the proposed control strategy is implemented in the PSIM environment and the simulation results are presented in Section V. Section VI concludes the paper.

II. LCC-COMPENSATED PICKUP

The pickup topology considered in this paper is shown in

Fig. 1. It consists of an LCC-compensated pickup [13] cascaded by a passive diode bridge that is used to rectify the voltage v_R to properly supply the battery V_B. Between them the switch S is inserted to control the charging battery current I_B. When the switch S is open, the rectifier output current i_o flows through the diode D and then is filtered by the capacitor C_{DC} and by the inductor L_{DC} prior to charging the battery. When the switch is closed it forms a short circuit at the rectifier output terminals and the resonating current i_R flows into it through the diodes D_1 and D_4 when it is positive, in diodes D_3 and D_2, alternatively. During this period, the battery current is provided by the capacitor C_{DC}. The rectifier output can be shorted because of the current-source characteristic of the LCC network. As regards the resonant tank, it is formed by the capacitor C_P in series with the pickup inductance L_P, by the rectifier-side inductance L_R and by the capacitor C. The capacitor C_P has the twofold purpose of: i) compensate part of the inductance L_P and ii) block the dc-component that can arise in the current i_P, thus avoiding the possible saturation of the ferrite core of the pickup coil. The inductance L_P is never fully compensated and so the LCC network behaves like an LCL circuit. The inductance L_R is set to be equal to the equivalent series inductance of the "P" branch and both resonate with the capacitor C. The resistances r_P and r_R account for the losses in the compensation network. The pickup circuitry is fed by the voltage v_P that is induced by the track current. Since the track current is sinusoidal with a controlled amplitude, the voltage v_P is also sinusoidal and its amplitude is given by:

$$V_P = \omega M I_T = \omega\, k\sqrt{L_T L_P}\, I_T \tag{1}$$

where ω and I_T are, respectively, the angular frequency and the magnitude of the track current. The parameter M is the mutual inductance between the track and the pickup coil that can be written in terms of coupling coefficient k as in the second of (1). From (1), it is easy to see that when the angular frequency and the magnitude of the track current are fixed, the magnitude of pickup induced voltage is proportional to k, provided that the track inductance L_T and the pickup inductance L_P remain unaffected by the variation of their relative position.

III. Pickup Operation

To study the operation of the circuit in Fig. (1), it is assumed that the rectifier works in the Continuous Conduction Mode (CCM), namely the current i_R never ceases to flow during the entire supply period. Under this assumption, the Fundamental Harmonics Approximation (FHA) analysis can provide good insight into the resonant LCC circuit operation [14]. FHA considers the ac quantities of the resonant tank as purely sinusoidal so that the circuit can be studied in the phasor-domain.

A. LCC Compensation Network

The previous considerations lead to rely on the circuit in Fig. 2 to study the behavior of the compensation network of the proposed pickup topology. Under the sinusoidal steady-state condition, the series of the pickup inductance and the capacitance C_P can be conceived as an equivalent inductor whose inductance is given by:

$$L = L_P - \frac{1}{\omega^2 C_P} \tag{2}$$

From the steady-state point of view, the LCC compensation is nothing else but the LCL circuit. As it is known from [15], when the capacitor C is designed in order to resonate with L at the chosen operating frequency, the current phasor $\bar{I}_R$ becomes independent from the voltage phasor $\bar{V}_R$ and, neglecting the small resistances r_P and r_R, can be expressed as:

$$\bar{I}_R = \frac{\bar{V}_P}{j\omega L} \tag{3}$$

If the rectifier-side inductance L_R is equal to the inductance L, the LCL network becomes symmetrical and, with the same hypotheses done in the derivation of (3), the phasor $\bar{I}_P$ of the pickup current can be obtained as:

$$\bar{I}_P = -\frac{\bar{V}_R}{j\omega L} \tag{4}$$

It is worth to note that pickup current is originated only by the voltage v_R. Since v_R depends mainly on the load, ideally, when there is no load, the pickup current vanishes.

An important requirement to satisfy in the pickup design is to achieve the UPF between the voltage v_P and the current i_P. This limits the pickup sizing factor and increases the system efficiency. The phase displacement between the pickup current and voltage can be assessed from the phase of the pickup input impedance which, from (4), can be written as:

$$\dot{Z}_P = \frac{\bar{V}_P}{\bar{I}_P} = -j\omega L \frac{\bar{V}_P}{\bar{V}_R} \tag{5}$$

Voltage v_P and current i_P are in phase when $\dot{Z}_P$ is real, i.e. when the load seen by the voltage source $\bar{V}_P$ is resistive. Equation (5) states that the angle of $\dot{Z}_P$ is zero if $\bar{V}_R$ lags $\bar{V}_P$ of 90°. By (3), this condition implies that $\bar{V}_R$ should be in phase with $\bar{I}_R$ to achieve the UPF of the pickup; the rectifier, the switch S with its control strategy and the battery of Fig. 1 have

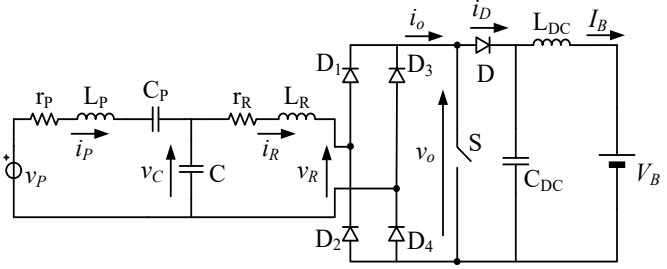

Fig. 1. Analyzed pickup topology.

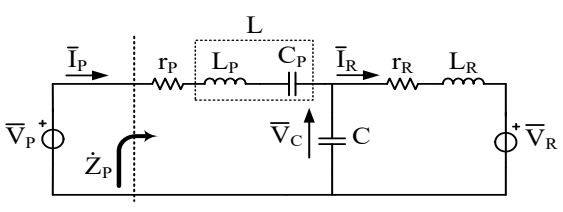

Fig. 2. LCC compensation network.

to appear as a resistance to the resonant tank.

B. *Proposed Control Strategy*

Although the amplitude of the phasor $\bar{I}_R$ can be directly derived from the phasor of the sinusoidal voltage induced in the pickup coil, as expected from (3), the computation of (4) requires the knowledge of the phasor $\bar{V}_R$ related to the fundamental $v_{R,1}$ of the rectifier input voltage v_R. The voltage v_R is influenced by the rectifier functioning that, in turn, depends on the battery operation and on the control strategy of the switch S. The rectifier input voltage for the circuit in Fig. 1 is neither sinusoidal nor a square wave, as it normally happens for the conventional pickup topologies, thus a time-domain analysis of the rectifier operation is required.

The time-domain analysis of the rectifier operation is based on the assumption that i_R is sinusoidal. The waveforms of the quantities affected by the proposed control strategy are ideally depicted in Fig. 3. The control signal v_g provided to the gate of the switch S is synchronized with the current i_R. For this reason, in Fig. 3 the origin of the angular coordinate θ, has been chosen in order to coincide with the negative to positive zero-crossing of the rectifier input current. In this reference system and with the above assumption, the rectifier input current can be written as:

$$i_R = I_R \sin(\theta) \tag{6}$$

From Fig. 3, it can be seen that in the interval [0, α] the switch S is on. During this period the rectifier output current i_o, obtained from the rectification of the current i_R, flows entirely through S and consequently, the current in the diode D is zero. The battery current I_B is provided by the capacitor C_{DC}. At θ=α, the switch S is turned off, the diode D starts conducting and the battery current is sustained by current i_D conveniently filtered. This situation persists until θ reaches the value (2π-α) when the switch S is turned on. During the interval [(2π-α), 2π], the current in the switch S, the current in the diode D and the battery current flow as in the period [0, α]. From the last graph of Fig. 3, it can be noticed that the battery current I_B is almost constant and it is obtained by filtering the current i_D. For this reason, the value of the constant I_B can be assessed from the average value of the current i_D which is given by:

$$I_D = I_B = \frac{1}{\pi}\int_{\alpha}^{\pi} I_R \sin(\theta)\, d\theta = \frac{2}{\pi} I_R \cos^2\left(\frac{\alpha}{2}\right) \tag{7}$$

In (7), the particular symmetry of the current i_D and the fact that it coincides with the current i_R in the interval [α, π] have been exploited. Equation (7) states that the battery charging current is independent from the battery voltage and it can be controlled by changing α, i.e. by changing the fraction of the overall period 2π in which the switch S is in the on-state. In other words, this pickup topology acts as a controlled current source, as long as the higher order harmonics in the rectifier current can be neglected.

As regards the voltage v_R, it can be noticed from the third plot of Fig. 3 that when the switch S is in the on-state, the voltage across the rectifier input terminals is clamped to zero. This is true provided that the voltage drops across the diodes of the rectifier and across the switch S are neglected. When the

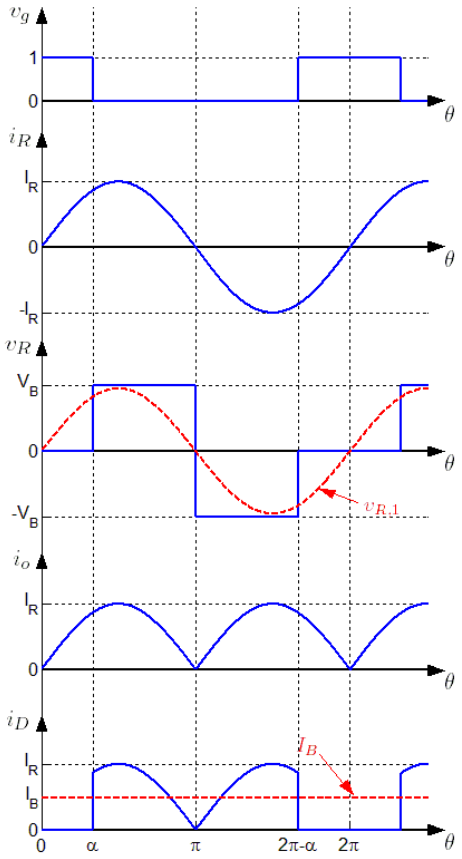

Fig. 3. Ideal waveforms of the quantities affected by the proposed control strategy. From top to bottom: i) gate signal of the switch S, ii) rectifier input current i_R, iii) rectifier input voltage v_R and its fundamental, iv) rectifier output current i_o, v) current i_D in the diode D and battery current I_B.

switch S is off the voltage v_R depends on the sign of i_R: it is equal to $+V_B$ when i_R is positive, to $-V_B$ conversely. In the third plot of Fig. 3, it is also shown that with the proposed control strategy the fundamental of the rectifier input voltage, depicted with the red dashed line, is ideally in phase with the current i_R. The amplitude of $v_{R,1}$ can be obtained from the Fourier series expansion of the signal v_R or more conveniently from power considerations. Considering the diode rectifier, the switch, the power diode, the capacitor C_{DC} and the inductance L_{DC} lossless components, the battery charging power should be equal to the ac active power seen by the rectifier input. The battery charging power is simply given by the battery current (7) multiplied by the battery voltage V_B and results:

$$P_B = V_B I_B = \frac{2}{\pi} V_B I_R \cos^2\left(\frac{\alpha}{2}\right) \tag{8}$$

The active power seen by the rectifier input is given by:

$$P_R = \frac{1}{2}\Re e[\bar{V}_R \bar{I}_R^*] = \frac{1}{2} V_R I_R \tag{9}$$

where the operator $\Re e[\cdot]$ extracts the real part from the complex number $\bar{V}_R \bar{I}_R^*$, which is the product between the phasor of the fundamental of v_R and the complex conjugate of the phasor $\bar{I}_R$. The second equality of (9) is derived from the fact that $v_{R,1}$ is in phase with i_R. In case of ideal components, the

battery charging power P_B is the same as P_R and, from (8) and (9), the amplitude of the fundamental of v_R can be obtained in the form:

$$V_R = \frac{4}{\pi} V_B \cos^2\left(\frac{\alpha}{2}\right) \tag{10}$$

Since with the proposed control method the voltage $v_{R,1}$ is always in phase with the current i_R, namely 90° lagging the voltage v_P, the impedance seen by the pickup voltage source expressed by (5) is pure resistive and this entails that the pickup does not have to cope with the reactive power.

IV. Pickup Design

The design of the pickup topology presented in this paper concerns with the sizing of the parameters of the LCC compensation network. Since the pickup inductance is essentially defined by geometrical constraints during the coil coupling design, the capacitor C_P allows a degree of freedom in the choice of L in order to adapt the rectifier output current to the battery demands. In fact, combining (3) and (7), the current that the converter is able to provide to charge the battery without the switching operation, i.e. with α equal to 0, can be written as:

$$I_D = I_o = \frac{2}{\pi} \frac{V_P}{\omega L} \tag{11}$$

It is easy to note that the average value of the rectifier output current I_o depends on the value of the inductance L and assumes the shape of the amplitude of the pickup induced voltage profile. With a constant amplitude and frequency of the track current and with a fixed value of the inductances L_T and L_P, from (1) it can be noticed that the pickup voltage profile depends on the coupling coefficient k, namely depends on the track and pickup structures and on their relative position. In this paper, a trapezoidal coil coupling profile versus the relative position between the pickup and the track coil is considered. This trapezoidal shape is a good approximation of the coil coupling profile achieved with the track structure introduced in [5]. From (1) and (11), the average value of the rectifier output current assumes also a trapezoidal shape and the resulting waveform is shown in Fig. 4. In addition to the current I_o, Fig. 4 illustrates also the average value of the power diode current, obtained operating the switch S in order to feed the battery with the proper current. Both the waveforms are plotted versus the relative position between the pickup coil and the track segment. This position is expressed through the variable x that starts from 0 when the pickup is approaching the track and is equal to the track length L when the car is leaving. If the car equipped with the pickup moves with constant speed, the x-axis can be also envisaged as the time variable. It is worth to note that the time scale of the plot in Fig. 4 is much greater than the period of the track current, i.e. the period of the waveforms of Fig. 3. For this reason, the equations found in the previous Section are still valid. From Fig. 4, it is easy to see an advantage of the LCC topology with respect to the series compensation in the pickup side. Indeed, at very low k, even though the current I_o at the rectifier output is less than the maxium current $I_{o,M}$ achievable when the pickup coil is well coupled with the track segment, it never ceases. Contrarily, in a series compensated pickup, when there is an high misanlignment between the track and the pickup, the rectifier output current is discontinuous and the power transfer becomes intermittent [16].

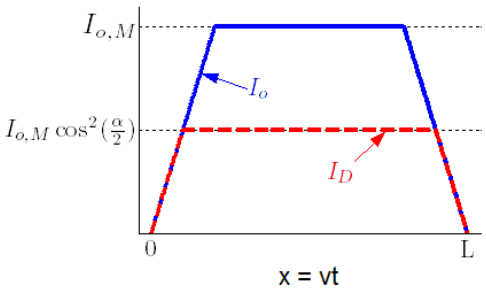

Fig. 4. Profile of the currents I_o and I_D when the pickup coil passes over a track segment.

When the battery is charging with the nominal current $I_{B,N}$, a good design of the LCC network makes the control operate with the minimum angle α, ideally 0. This is achieved forcing the quantity $I_{o,M}$, obtained with (1) and (11) when k is set to the maximum value k_M, to be equal to the battery nominal current. This yields the value for the inductance L:

$$L = \frac{2}{\pi} \frac{1}{\omega} \frac{V_{P,M}}{I_{B,N}} \tag{12}$$

where $V_{P,M}$ is the maximum value of the amplitude of the pickup induced voltage, which gives rise to the maximum value $I_{o,M}$ for the average value of the rectifier output current. The value of the inductance in (12) has to be used to size L_R. It can happen that this value is too small to mitigate the harmonics in the current i_R introduced by the voltage v_R. To face this problem, the inductance L_R can be replaced with the series of an inductor and a capacitor; the inductor has a value higher than the one obtained with (12) and the capacitor is designed to partially compensate it in order to see an equivalent inductance whose value is L at the supply frequency. The resulting modified LCC circuit is sketched in Fig. 5a. The inductance L_R can be designed in order to fix the maximum value of the 2-nd order harmonic $I_{R,2}$ of the current i_R as a percentage of the fundamental I_R. To find the value of $I_{R,2}$, the scheme in Fig. 5b can be examined. It is used to assess the relations between the n-th harmonics of the quantities in the compensation network of the proposed topology; for this reason, the pure sinusoidal pickup voltage does not appear in it. All the reactances of Fig. 5b are expressed as function of the harmonic order n. For example, the reactance associated to the capacitor C at frequencies multiple of the nominal one ω is given by:

$$X_{C,n} = -\frac{1}{n\omega C} = -\frac{\omega L}{n} \tag{13}$$

in which the last equality holds because the capacitor C is designed to resonate with L at the nominal frequency. The equivalent reactances X_P and X_R have a similar expression which is found to be:

$$X_{i,n} = n\omega L_i - \frac{1}{n\omega C_i} = \left(\frac{n^2-1}{n}\right)\omega L_i + \frac{\omega L}{n} \tag{14}$$

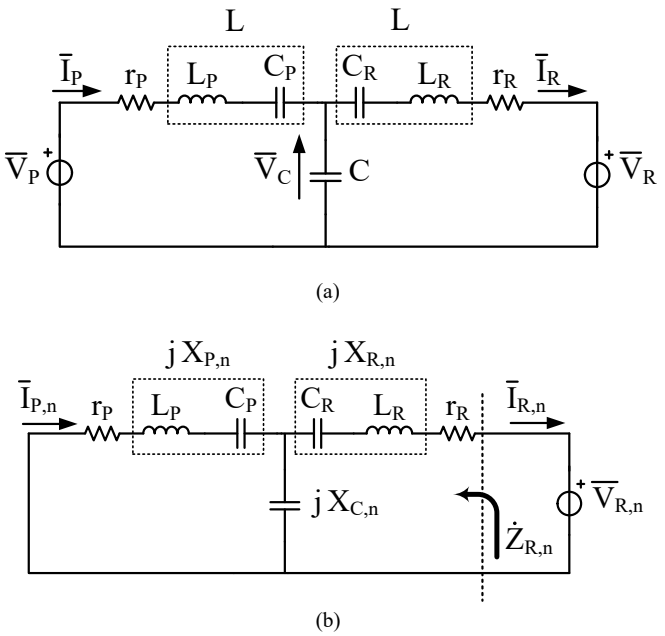

Fig. 5. Modified LCC compensation network. Circuit for the analysis of the fundamental quantities (a) and for the n-th order harmonics (b). n=2,3,4…

where the subscript i=P,R indicates either the "P" or the "R" branch. In the derivation of (14) the expression (2) has been exploited to substitute for C_P. An equivalent equation holds for C_R. The n-th harmonic of the current i_R is given by:

$$I_{R,n} = \frac{V_{R,n}}{Z_{R,n}} \tag{15}$$

where the quantity $V_{R,n}$ is the amplitude of the n-th harmonic of v_R and $Z_{R,n}$ is the magnitude of the output impedance indicated in Fig. 5b. The calculation of the impedance $\dot{Z}_{R,n}$ can be approximated considering $|X_{C,n}|$ small with respect to the reactance $X_{P,n}$; this is a valid approximation because usually L_P is greater that L. With this hypothesis, the harmonics of the current i_R do not flow in the "P" branch and, neglecting the small resistance r_R, the impedance $\dot{Z}_{R,n}$ becomes:

$$\dot{Z}_{R,n} \cong j\left(X_{R,n} + X_{C,n}\right) = j\left(\frac{n^2-1}{n}\right)\omega L_R \tag{16}$$

To calculate the 2-nd order harmonic of the current i_R, it is necessary to know $V_{R,2}$ that can be evaluated from the absolute value of the relative Fourier coefficient of the voltage v_R shown in the third plot of Fig. 3. It is given by:

$$V_{R,2} = \left|\frac{2}{\pi}\int_{\alpha}^{\pi} V_B \sin(2\theta)\, d\theta\right| = \frac{2}{\pi} V_B \sin^2(\alpha) \tag{17}$$

From (17), it can be noticed that the maximum value of the 2-nd harmonic of the rectifier input voltage is achieved when α is equal to $\frac{\pi}{2}$ and its value is $\frac{2}{\pi}V_{B,M}$ where $V_{B,M}$ is the maximum battery voltage. Substituting n=2 in (16) and using (15) and (17), the maximum value of the 2-nd order harmonic of the current i_R is:

$$I_{R,2} = \frac{4}{3\pi}\frac{V_{B,M}}{\omega L_R} \tag{18}$$

The value of L_R can be obtained by imposing that the ratio between the amplitudes of the 2-nd harmonic and the fundamental of i_R is equal to a small fraction, for example 0.1. This leads to the equation:

$$\frac{I_{R,2}}{I_R} = 0.1 \;\Rightarrow L_R = 10\,\frac{4}{3\pi}\frac{V_{B,M}}{V_{P,M}}L \tag{19}$$

In the derivation of (19), the current I_R has been obtained using (3) with the maximum induced pickup voltage. It is worth to note that the harmonic content of the current i_R depends on the ratio $\frac{V_B}{V_{P,M}}$ that cannot be too high to avoid an oversizing of the inductance L_R.

Based on these considerations the design of the parameters of the modified LCC compensation network can be summarized as follow:

- Given the maximum pickup induced voltage $V_{P,M}$ and the nominal battery current $I_{B,N}$, the value for the inductance L can be found with (12).
- The capacitor C that resonates with L at the nominal frequency is given by $C = \frac{1}{\omega^2 L}$.
- With a given maximum battery voltage, the inductance L_R can be calculated according to (19).
- The capacitance C_P is derived from (2) and an equivalent equation is used for sizing C_R.

V. Simulation Results

The circuit of Fig. 1 with the modified LCC structure of Fig. 5a has been implemented in the PSIM environment. The DWPTS, intended to charge a battery with a nominal current $I_{B,N}$ of 25 A and a nominal voltage $V_{B,N}$ of 296 V, has been designed around the specifications listed in the upper part of the Table I and according to the procedure explained in the previous Section. The selection of the capacitor C_{DC} and the inductance L_{DC} has been based on considerations regarding voltage and current ripple attenuation. The resulting components ratings can be found in the lower part of the Table I. The small value of the inductance L_{DC} required to mitigate the battery current ripple is worth noting. The inductance L of Table I has been chosen less than 19 µH, value given by (12). This safety margin guarantees the battery charging with the nominal current $I_{B,N}$ even with the presence of the resistances

Tab. I. Specifications and Components Ratings of the Simulated Circuit

Specifications			
Parameter	Value	Parameter	Value
$V_{P,M}$	400 V	I_B	2.5÷25 A
ω	2π·85000 rad/s	V_B	240÷336 V
Component Ratings			
L	17 µH	C	206 nF
L_P	120 µH	C_P	34 nF
L_R	60 µH	C_R	82 nF
L_{DC}	5 µH	C_{DC}	300 µF
r_P	0.2 Ω	r_R	0.1 Ω

r_P and r_R, neglected in the theoretical analysis. With this selection of L, the output current I_o expected from (11) is about 28 A. To control the battery charging, a battery current loop that provides the control angle for the switch S has been implemented. The nominal control angle α_N, which would have been 0 in ideal conditions if the outcome of (12) had used to design L, from (7) is found to be around 0.67 rad and 0.57 rad from simulation (a similar value can be obtained employing cumbersome equations that take into account r_P and r_R). To confirm the analysis done in Section III, Fig. 6 reports the currents i_D and I_B obtained simulating the circuit of Fig. 1 under nominal conditions and when the coupling coefficient is maximum. The waveforms of Fig. 6 are in good agreement with the last plot of Fig. 3 apart from the small variations in the amplitude of current i_D that are caused by the harmonics introduced in the LCC network by the voltage v_R. These harmonics are emphasized during the constant voltage charging mode, for example when the battery absorbs half of the maximum power. In this situation, the battery charging current is 12.5 A with an ideal control angle α equal to 1.68 rad obtained from (7). These harmonics affect a little bit the phase displacement between the pickup induced voltage and the pickup current, as can be seen from Fig. 7. The pickup current (red line marked with crosses) is leading the voltage v_P (blue line without marks) by a small angle. As a comparison, the topology and the control strategy introduced in [11] have been simulated with the same parameters and under the half-load condition. The resulting pickup current is shown in Fig. 7 with a black line marked with dots. In this case, the current lags the voltage of about 47° and its amplitude is about 40% higher with respect to the amplitude of the pickup current obtained with the circuit analyzed in this paper, which can attain higher efficiencies.

VI. Conclusions

The paper proposes a different topology for the dc/dc converter downstream a modified version of an LCC-compensated pickup for a DWPTS. This topology does not rely on a bulky dc-side inductance for the proper operation and the adopted control strategy allows a UPF to be maintained at the pickup ac input stage. The pickup operation has been studied analytically and a design method for the LCC circuit has been introduced. Computer simulations confirm the analytical analysis and show the better performance in terms of input UPF of this topology with respect to a similar one.

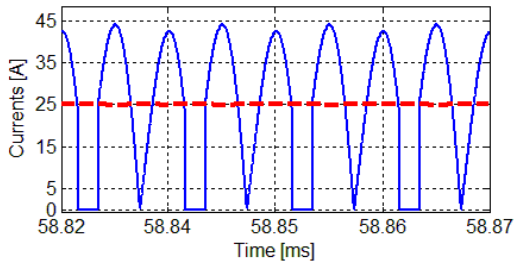

Fig. 6. Current i_D(blue solid) and i_B (red dashed) in nominal conditions obtained from simulation.

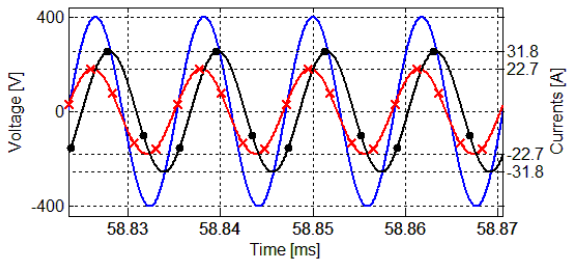

Fig. 7. Pickup voltage v_P (blue without marks) and current i_P (red marked with crosses) from the simulation of the half-load condition. For the same condition, the current i_P (black marked with dots) obtained with the topology and the control strategy presented in [11].

Acknowledgement

M. Forato would like to thank the interdepartmental Center "Giorgio Levi Cases" for supporting his Ph.D. grant.

References

[1] S. S. Williamson, A. K. Rathore and F. Musavi, "Industrial electronics for electric transportation: current state-of-the-art and future challenges," *IEEE Trans. Ind. Electron.*, vol. 62, no. 5, pp. 3021-3032, May 2015.

[2] C. C. Mi, G. Buja, S. Y. Choi and C. T. Rim, "Modern advances in wireless power transfer systems for roadway powered electric vehicles," *IEEE Trans. Ind. Electron*., vol. 63, no. 10, pp. 6533-6545, Oct. 2016.

[3] M. Yilmaz, V. T. Buyukdegirmenci and P. T. Krein, "General design requirements and analysis of roadbed inductive power transfer system for dynamic electric vehicle charging," in *Proc. 2012 IEEE Transport. Electrif. Conf. Expo (ITEC)*, 2012, pp. 1-6.

[4] G. Buja, M. Bertoluzzo and H. K. Dashora, "Lumped track layout design for dynamic wireless charging of electric vehicles," *IEEE Trans. Ind. Electron.*, vol. 63, no. 10, pp. 6631-6640, Oct. 2016.

[5] G. R. Nagendra, G. A. Covic and J. T. Boys, "Sizing of inductive power pads for dynamic charging of EVs on IPT highways," *IEEE Trans. Transport. Electrif.*, vol. 3, no. 2, pp. 405-417, June 2017.

[6] R. Bosshard, U. Badstübner, J. W. Kolar and I. Stevanović, "Comparative evaluation of control methods for inductive power transfer," in *Proc. 2012 Int. Conf. Renewable Energy Res. Appl. (ICRERA)*, 2012, pp. 1-6.

[7] G. Lovison, M. Sato, T. Imura and Y. Hori, "Secondary-side-only simultaneous power and efficiency control for two converters in wireless power transfer system," in *Proc. 41st Annu. Conf. IEEE Ind. Electron. Soc. (IECON)*, 2015, pp. 004824-004829.

[8] H. H. Wu, A. Gilchrist, K. D. Sealy and D. Bronson, "A high efficiency 5 kW inductive charger for EVs using dual side control," *IEEE Trans. Ind. Informat.*, vol. 8, no. 3, pp. 585-595, Aug. 2012.

[9] M. Fu, C. Ma and X. Zhu, "A cascaded boost–buck converter for high-efficiency wireless power transfer systems," *IEEE Trans. Ind. Informat.,* vol. 10, no. 3, pp. 1972-1980, Aug. 2014.

[10] U. K. Madawala and D. J. Thrimawithana, "A bidirectional inductive power interface for electric vehicles in V2G systems," *IEEE Trans. Ind. Electron.*, vol. 58, no. 10, pp. 4789-4796, Oct. 2011.

[11] C. Y. Huang, J. T. Boys and G. A. Covic, "LCL pickup circulating current controller for inductive power transfer systems," *IEEE Trans. Power Electron.*, vol. 28, no. 4, pp. 2081-2093, Apr. 2013.

[12] N. A. Keeling, G. A. Covic and J. T. Boys, "A unity-power-factor IPT pickup for high-power applications," *IEEE Trans. Ind. Electron.*, vol. 57, no. 2, pp. 744-751, Feb. 2010.

[13] S. Li, W. Li, J. Deng, T. D. Nguyen and C. C. Mi, "A double-sided LCC compensation network and its tuning method for wireless power transfer," *IEEE Trans. Veh. Technol.*, vol. 64, no. 6, pp. 2261-2273, June 2015.

[14] A. Safaee and K. Woronowicz, "Time-domain analysis of voltage-driven series–series compensated inductive power transfer topology," *IEEE Trans. Power Electron.*, vol. 32, no. 7, pp. 4981-5003, Jul. 2017.

[15] M. Borage, S. Tiwari, and S. Kotaiah, "Analysis and design of an LCL-T resonant converter as a constant-current power supply," *IEEE Trans. Ind. Electron.*, vol. 52, no. 6, pp. 1547–1554, Dec. 2005.

[16] M. Bertoluzzo, G. Buja and H. K. Dashora, "Design of DWC system track with unequal DD coil set," *IEEE Trans. Transport. Electrific.*, vol. 3, no. 2, pp. 380-391, June 2017.